Transfer matrix analysis of the unidirectional grating-assisted codirectional coupler

Brian R. West* and David V. Plant

Department of Electrical and Computer Engineering, Photonic Systems Group, McGill University, Montreal, Quebec H3A 2A7, Canada

*Corresponding author: Brian.West@mail.mcgill.ca

Received 15 August 2007; revised 26 September 2007; accepted 15 October 2007; posted 15 October 2007 (Doc. ID 86501); published 19 November 2007

The unidirectional grating-assisted codirectional coupler (U-GACC) has recently been proposed. This unique structure permits irreversible coupling between orthogonal waveguide eigenmodes by means of simultaneous modulation of both the real and imaginary parts of the refractive index in the coupling region. Analysis of the U-GACC has until now relied on coupled mode theory, which can be restrictive in its application as a design tool. We analyze the U-GACC by the transfer matrix method, which demonstrates in a simple fashion why the device operates in a unidirectional manner. In addition, we show that for all practical designs, there is a limit to the minimum cross talk between outputs, a phenomenon that has not been previously identified. © 2007 Optical Society of America

OCIS codes: 060.1810, 130.3120, 250.4480.

1. Introduction

Grating-assisted couplers (GACs) form the basis for a variety of photonic devices [1,2]. In a GAC, power transfer between orthogonal waveguide eigenmodes p and q is achieved using a longitudinal refractive index perturbation in a region where the mode fields overlap [3]; the coupling strength from mode p to mode q is equal to that from mode q to mode p, a condition known as *reciprocal coupling*. In general, GACs can couple power between forward- and backward-propagating modes (Bragg grating), or between forward-propagating modes in multimode or parallel asynchronous single-mode waveguides (long-period grating). In the former, the equal coupling strength results in an exponentially decaying power profile along the length of the grating, while in the latter, the profile is sinusoidal, requiring greater modeling precision in order to determine the optimal grating parameters.

Recently, there has been significant interest in a variation of the GAC that exhibits unidirectional power transfer [4,5]. Here, the term "unidirectional" does not refer to the physical direction of power flow, but rather to the unique phenomenon whereby power may be coupled from mode p to mode q but not from mode q to mode p. This type of coupling has also been referred to as "irreversible" and "nonreciprocal." We choose to avoid these terms in order to prevent confusion with the common but unrelated concept of Faraday isolation. These unidirectional coupling structures show great promise in optical routing and computing as a lossless add multiplexer [6] and as an optical memory cell [7,8].

Despite the vast potential for these devices, very little progress has been made in their design and analysis. The earliest known description of a unidirectional GAC used resonance mode expansion to derive the unidirectional coupling properties [9], and all subsequent analyses have used coupled mode theory (CMT) [6,10,11]. While it is an important pedagogical tool, CMT is known to be inaccurate for precise design work. Errors can be particularly severe in the case of large index perturbations, or—in the case of corrugated gratings—when the grating teeth project in a direction parallel to the electric field polarization vector of the modes. For vertical slab couplers this is the TM polarization. In the case of in-plane coupling, either or both polarizations are affected—and to different degrees—depending on the grating geometry used [12]. In either case, the perturbations in mode

0003-6935/07/338052-09$15.00/0

profiles within each grating period are not accounted for in CMT, and this leads to erroneous results when calculating the optimal period and duty cycle.

In this work, we analyze an ideal unidirectional GAC by the well-known transfer matrix method (TMM). While we consider only the unidirectional grating-assisted codirectional coupler (U-GACC) utilizing a long-period grating, the methods discussed here are equally applicable to Bragg gratings. Section 2 contains a general description of the U-GACC, and describes the conditions for its ideal operation. In Section 3, the single-period transfer matrix is derived, and is found to exhibit a strong asymmetry between the off-diagonal elements, indicating that the power transfer is indeed unidirectional. A simple expression is found for the number of grating periods required for power equalization in each mode, and it is shown that there is a fundamental limitation to the minimum cross talk, defined here as the ratio of power coupled in the forbidden direction to power coupled in the allowed direction. Section 4 contains an example of the U-GACC, where the TMM is confirmed by comparison with beam propagation method simulations.

2. Description of the U-GACC

A real index grating, $\Delta n(z) = n_0 \sin(2\pi z/\Lambda)$, consists of a sinusoidal index perturbation of amplitude n_0 and period Λ (periodic but nonsinusoidal gratings can be decomposed into a superposition of sinusoidal components, of which we consider only one to contribute to the coupling of modes p and q). When the difference in modal propagation constants is equal to the grating vector K_g,

$$\beta_p - \beta_q = K_g = 2\pi/\Lambda, \tag{1}$$

maximum power transfer can be obtained. In the spatial frequency domain, a pure index grating exhibits dual sidebands at $\pm K_g$, as the Fourier power spectrum of a real function is symmetric. By Eq. (1), this equalizes the coupling strength between modes p and q.

Unidirectional coupling requires a grating with only a single sideband. This is accomplished through the use of a complex grating,

$$\Delta n(z) = n_0 \exp(\pm i K_g z) = n_0[\cos(K_g z) \pm i \sin(K_g z)]. \tag{2}$$

From Eq. (2) it is apparent that in order to achieve unidirectional coupling, a grating is required in which both the real refractive index and the gain–loss coefficient are modulated with identical amplitudes and relative phase of $\pm\pi/2$. The sign of the phase difference determines the sole direction of coupling; from Eq. (1), a positive sign allows coupling from the mode with higher β to the mode with lower β. As with all grating-based devices, ideal operation exists at a nominal operating wavelength, from which detuning will alter the phase-matching condition described in Eq. (1). In this work, we examine the ideal case only; nonidealities such as wavelength detuning, phase offset, and nonidentical grating amplitudes will be examined in a future work.

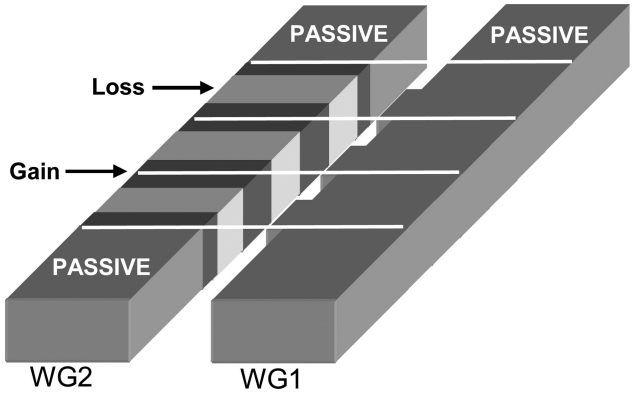

Fig. 1. Asynchronous coupler embodiment of the U-GACC (three periods shown). The real index grating is in waveguide 1 (WG1) and the gain–loss grating is in waveguide 2 (WG2). White lines are drawn to show each grating period, indicating the $\pm\pi/2$ phase offset between the gratings.

One possible embodiment of the U-GACC incorporates an asynchronous directional coupler, and is shown in Fig. 1. Here, the real grating exists as a corrugation in one passive waveguide (WG1) while the gain–loss grating exists in a parallel waveguide of different propagation constant (WG2). The regions of WG2 preceding and following the gain–loss grating are passive. Such a waveguide could in principle consist of an active waveguide that is sectionally pumped at three different levels: high (for gain), medium (for transparency), and low (for loss). The waveguides are in close enough proximity that when considered together as a single waveguiding system, they support two orthogonal supermodes, which closely resemble the modes of each isolated waveguide [6].

A second embodiment of the U-GACC utilizes a dual-mode waveguide as shown in Fig. 2. In this figure, the real and imaginary gratings are spatially colocated, although this is not necessary. As the interacting modes of the unperturbed waveguide exhibit even and odd symmetry, the gratings exist in just half of the waveguide cross section in order to

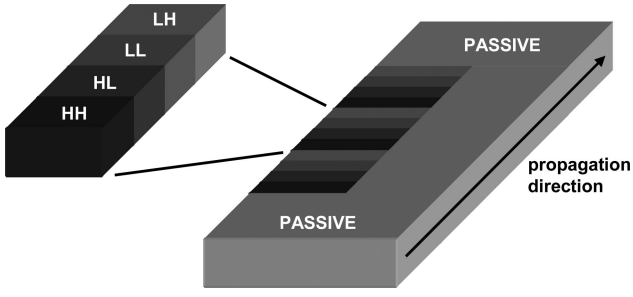

Fig. 2. Dual-mode waveguide embodiment of the U-GACC (three periods shown). Both gratings coexist within one half of the waveguide cross section. Inset, one period of the grating, with the labeling used in this paper.

produce a finite coupling between modes. In practice, the two modes can be spatially (de)multiplexed by an asymmetric adiabatic y-branch coupler [13]. The structure in Fig. 2 shall be considered in the remainder of this work.

3. Analysis by Transfer Matrix Method

For our analysis, we assume that there are only two guided modes present. In the case that more than two guided modes exist, this analysis is still valid if the Fourier decomposition of the complex grating includes only spatial frequencies that are matched to the difference in propagation constants of the relevant modes. Additionally, we assume that the grating is piecewise continuous rather than sinusoidal, which is generally the case for long-period gratings.

As a test case, we consider the U-GACC shown in Fig. 2, in which the gain–loss grating leads the index grating in the propagation direction. Based on the discussion in Section 2, we expect this structure to allow coupling from the mode with lower β to that with higher β (that is, from the odd mode to the even mode). From this figure, it is apparent that the U-GACC consists of a periodic repetition of four different grating segments, as opposed to just two in the case of a piecewise continuous real index grating. These segments are labeled RI (R, I = "H," "L") to indicate whether the real (R) and imaginary (I) parts of the index perturbation are higher or lower than the average index, respectively. In the TMM, the complex amplitudes of the modes are tracked via two-by-two matrices as they propagate within each segment of the grating, and as they scatter at the grating planes. In this fashion, the transfer matrix of one full period of the grating is described by a matrix $\mathbf{T}$, and that of the entire N-period grating structure is described by the matrix $\mathbf{T}^N$. Electric field mode amplitudes are easily calculated as $\mathbf{E}_{\text{out}} = \mathbf{T}^N\mathbf{E}_{\text{in}}$, or

$$\begin{bmatrix} E_1^{\text{out}} \\ E_2^{\text{out}} \end{bmatrix} = \mathbf{T}^N \begin{bmatrix} E_1^{\text{in}} \\ E_2^{\text{in}} \end{bmatrix}, \tag{3}$$

with magnetic field mode amplitudes defined analogously.

A. Description of the Mode Fields in an Ideal U-GACC

For most applications of the TMM, it suffices to simply obtain a numerical solution for the mode fields in each grating segment. In the case of the ideal U-GACC, we are interested in the relationship among these fields, and how this is manifested in the matrices that describe the structure. In particular, it is important to determine what constitutes real and imaginary gratings of *equal amplitude* as in Eq. (2); this is particularly important when these gratings are not spatially colocated in the xy plane. We begin by defining the index profile in each of the four grating segments in terms of an unperturbed profile $\tilde{n}(x, y)$ with both real and imaginary index perturbations,

$$n(x, y) = \tilde{n}(x, y) \pm \Delta n^R(x, y) \pm \Delta n^I(x, y), \tag{4}$$

where the signs of each perturbation depend on the particular grating segment. The spatial profiles and magnitudes of Δn^R and Δn^I need not be identical for the ideal U-GACC. Next, we define the modes p and q in each segment of the grating. These are necessarily complex-valued due to the presence of the gain–loss grating, and thus they cannot be normalized to carry unit power as is common in most TMM descriptions. Rather, they are orthonormalized in the sense that

$$\frac{1}{4}\iint (\mathbf{E}_p \times \mathbf{H}_q + \mathbf{E}_q \times \mathbf{H}_p)\mathrm{d}a = \delta_{pq} \tag{5}$$

in any given segment of the grating, where

$$\delta_{pq} = \begin{cases} 1, & p = q \\ 0, & p \neq q \end{cases} \tag{6}$$

is the Kronecker delta symbol and $\mathrm{d}a = \hat{z}\mathrm{d}x\mathrm{d}y$ is the differential element of cross-sectional area perpendicular to the direction of propagation. Here and throughout this work, we suppress the transverse spatial coordinates (x, y) of all fields for brevity. In Subsection 3.B, we shall define the elements of the transfer matrices in an analogous fashion, but with modes p and q existing in the grating segments following and preceding the grating plane under examination, respectively.

The mode fields in an arbitrary segment are equal to those in the unperturbed waveguide with small real and imaginary perturbations,

$$\begin{aligned} \mathbf{E}_{p,q} &= \tilde{\mathbf{E}}_{p,q} + \Delta\mathbf{E}_{p,q}{}^R + i\Delta\mathbf{E}_{p,q}{}^I, \\ \mathbf{H}_{p,q} &= \tilde{\mathbf{H}}_{p,q} + \Delta\mathbf{H}_{p,q}{}^R + i\Delta\mathbf{H}_{p,q}{}^I. \end{aligned} \tag{7}$$

Note that all perturbation fields $\{\Delta\mathbf{E}, \Delta\mathbf{H}\}$ as defined above are real-valued in order to simplify the following derivation. Similar to Eq. (5), we define an orthonormality relation for modes p and q in the unperturbed waveguide,

$$\frac{1}{4}\iint \left(\tilde{\mathbf{E}}_p \times \tilde{\mathbf{H}}_q + \tilde{\mathbf{E}}_q \times \tilde{\mathbf{H}}_p\right)\mathrm{d}a = \delta_{pq}, \tag{8}$$

and furthermore introduce the following auxiliary orthonormality relations, which arise from consideration of the real and imaginary perturbations separately:

$$\begin{aligned} \frac{1}{4}\iint &\left[\left(\tilde{\mathbf{E}}_p \pm \Delta\mathbf{E}_p{}^R\right) \times \left(\tilde{\mathbf{H}}_q \pm \Delta\mathbf{H}_q{}^R\right)\right] + \left[\left(\tilde{\mathbf{E}}_q \pm \Delta\mathbf{E}_q{}^R\right)\right. \\ &\left. \times \left(\tilde{\mathbf{H}}_p \pm \Delta\mathbf{H}_p{}^R\right)\right]\mathrm{d}a = \delta_{pq}, \end{aligned} \tag{9}$$

$$\begin{aligned} \frac{1}{4}\iint &\left[\left(\tilde{\mathbf{E}}_p \pm i\Delta\mathbf{E}_p{}^I\right) \times \left(\tilde{\mathbf{H}}_q \pm i\Delta\mathbf{H}_q{}^I\right)\right] + \left[\left(\tilde{\mathbf{E}}_q \pm i\Delta\mathbf{E}_q{}^I\right)\right. \\ &\left. \times \left(\tilde{\mathbf{H}}_p \pm i\Delta\mathbf{H}_p{}^I\right)\right]\mathrm{d}a = \delta_{pq}. \end{aligned} \tag{10}$$

Finally, we define the mode fields in each segment, to first order, as

$$\mathbf{E}_{p,q}^{HH} = \tilde{\mathbf{E}}_{p,q} + \Delta\mathbf{E}_{p,q}^{R} + i\Delta\mathbf{E}_{p,q}^{I},$$
$$\mathbf{H}_{p,q}^{HH} = \tilde{\mathbf{H}}_{p,q} + \Delta\mathbf{H}_{p,q}^{R} + i\Delta\mathbf{H}_{p,q}^{I}, \quad (11)$$

$$\mathbf{E}_{p,q}^{HL} = \tilde{\mathbf{E}}_{p,q} + \Delta\mathbf{E}_{p,q}^{R} - i\Delta\mathbf{E}_{p,q}^{I},$$
$$\mathbf{H}_{p,q}^{HL} = \tilde{\mathbf{H}}_{p,q} + \Delta\mathbf{H}_{p,q}^{R} - i\Delta\mathbf{H}_{p,q}^{I}, \quad (12)$$

$$\mathbf{E}_{p,q}^{LL} = \tilde{\mathbf{E}}_{p,q} - \Delta\mathbf{E}_{p,q}^{R} - i\Delta\mathbf{E}_{p,q}^{I},$$
$$\mathbf{H}_{p,q}^{LL} = \tilde{\mathbf{H}}_{p,q} - \Delta\mathbf{H}_{p,q}^{R} - i\Delta\mathbf{H}_{p,q}^{I}, \quad (13)$$

$$\mathbf{E}_{p,q}^{LH} = \tilde{\mathbf{E}}_{p,q} - \Delta\mathbf{E}_{p,q}^{R} + i\Delta\mathbf{E}_{p,q}^{I},$$
$$\mathbf{H}_{p,q}^{LH} = \tilde{\mathbf{H}}_{p,q} - \Delta\mathbf{H}_{p,q}^{R} + i\Delta\mathbf{H}_{p,q}^{I}. \quad (14)$$

B. Derivation of Transfer Matrices

We begin by defining the transfer matrix elements at the grating plane from segment RI to segment $R'I'$,

$$T_{pq}^{(R'I')RI} = \frac{1}{4}\int\int \left[\left(\mathbf{E}_p^{R'I'} \times \mathbf{H}_q^{RI}\right) + \left(\mathbf{E}_q^{RI} \times \mathbf{H}_p^{R'I'}\right)\right] \mathrm{d}\alpha. \quad (15)$$

Specifically, for propagation across an imaginary grating plane from segment HH to segment HL,

$$T_{pq}^{(HL)HH} = \frac{1}{4}\int\int \left[\left(\mathbf{E}_p^{HL} \times \mathbf{H}_q^{HH}\right) + \left(\mathbf{E}_q^{HH} \times \mathbf{H}_p^{HL}\right)\right] \mathrm{d}\alpha. \quad (16)$$

Inserting Eqs. (11) and (12) into Eq. (16), applying Eq. (9), and keeping only the lowest-order perturbation term produces the matrix elements

$$T_{11}^{(HL)HH} = 1 + \frac{1}{2}\int\int \left(\Delta\mathbf{E}_1^{I} \times \Delta\mathbf{H}_1^{I}\right) \mathrm{d}\alpha, \quad (17)$$

$$T_{22}^{(HL)HH} = 1 + \frac{1}{2}\int\int \left(\Delta\mathbf{E}_2^{I} \times \Delta\mathbf{H}_2^{I}\right) \mathrm{d}\alpha, \quad (18)$$

$$T_{21}^{(HL)HH} = -\frac{i}{2}\int\int \left[\left(\Delta\mathbf{E}_2^{I} \times \tilde{\mathbf{H}}_1\right) + \left(\tilde{\mathbf{E}}_1 \times \Delta\mathbf{H}_2^{I}\right)\right] \mathrm{d}\alpha, \quad (19)$$

$$T_{12}^{(HL)HH} = \frac{i}{2}\int\int \left[\left(\Delta\mathbf{E}_2^{I} \times \tilde{\mathbf{H}}_1\right) + \left(\tilde{\mathbf{E}}_1 \times \Delta\mathbf{H}_2^{I}\right)\right] \mathrm{d}\alpha. \quad (20)$$

The transfer matrix at this grating plane thus takes the form

$$\mathbf{T}^{(HL)HH} = \begin{bmatrix} 1 + \frac{\left(\varepsilon_1^{I}\right)^2}{2} & i\varepsilon_X^{I} \\ -i\varepsilon_X^{I} & 1 + \frac{\left(\varepsilon_2^{I}\right)^2}{2} \end{bmatrix}, \quad (21)$$

with

$$\left(\varepsilon_1^{I}\right)^2 = \int\int \left(\Delta\mathbf{E}_1^{I} \times \Delta\mathbf{H}_1^{I}\right) \mathrm{d}\alpha, \quad (22)$$

$$\left(\varepsilon_2^{I}\right)^2 = \int\int \left(\Delta\mathbf{E}_2^{I} \times \Delta\mathbf{H}_2^{I}\right) \mathrm{d}\alpha, \quad (23)$$

$$\varepsilon_X^{I} = \frac{1}{2}\int\int \left[\left(\Delta\mathbf{E}_2^{I} \times \tilde{\mathbf{H}}_1\right) + \left(\tilde{\mathbf{E}}_1 \times \Delta\mathbf{H}_2^{I}\right)\right] \mathrm{d}\alpha. \quad (24)$$

This notation is chosen in order to keep track of the perturbation order contained in each matrix element; the cross-coupling (off-diagonal) terms represent a first-order contribution of field perturbations, while the self-coupling (diagonal) terms represent a second-order contribution. We note further that all ε terms are real-valued. A similar derivation of the transfer matrix for propagation from segment LL to segment LH uses Eqs. (13) and (14), resulting in

$$\mathbf{T}^{(LH)LL} = \begin{bmatrix} 1 + \frac{\left(\varepsilon_1^{I}\right)^2}{2} & -i\varepsilon_X^{I} \\ i\varepsilon_X^{I} & 1 + \frac{\left(\varepsilon_2^{I}\right)^2}{2} \end{bmatrix} = \left(\mathbf{T}^{(HL)HH}\right)^T, \quad (25)$$

that is, the two imaginary transfer matrices are the nonconjugate transpose of each other.

For the real grating planes, using Eq. (10) rather than Eq. (9), the transfer matrices are

$$\mathbf{T}^{(LL)HL} = \begin{bmatrix} 1 - \frac{\left(\varepsilon_1^{R}\right)^2}{2} & \varepsilon_X^{R} \\ -\varepsilon_X^{R} & 1 - \frac{\left(\varepsilon_2^{R}\right)^2}{2} \end{bmatrix},$$
$$\mathbf{T}^{(HH)LH} = \left(\mathbf{T}^{(LL)HL}\right)^T, \quad (26)$$

with

$$\left(\varepsilon_1^{R}\right)^2 = \int\int \left(\Delta\mathbf{E}_1^{R} \times \Delta\mathbf{H}_1^{R}\right) \mathrm{d}\alpha, \quad (27)$$

$$\left(\varepsilon_2^{R}\right)^2 = \int\int \left(\Delta\mathbf{E}_2^{R} \times \Delta\mathbf{H}_2^{R}\right) \mathrm{d}\alpha, \quad (28)$$

$$\varepsilon_X{}^R = \frac{1}{2}\int\int \left[\left(\Delta \mathbf{E}_2{}^R \times \tilde{\mathbf{H}}_1\right) + \left(\tilde{\mathbf{E}}_1 \times \Delta \mathbf{H}_2{}^R\right)\right] \mathrm{d}a. \tag{29}$$

Comparing Eqs. (25) and (26), it is apparent that in the TMM picture, the condition of equal real and imaginary coupling strengths requires that

$$\left|\varepsilon_X{}^R\right| = \left|\varepsilon_X{}^I\right| \equiv |\varepsilon_X|. \tag{30}$$

We shall see later that the terms $(\varepsilon_{p,q}{}^{RI})^2$ fall out of the full-period transfer matrix.

C. Derivation of Propagation Matrices

Within each grating segment, both modes propagate independently along the z direction, accumulating a phase

$$\phi_{p,q}{}^{RI}(z) = \beta_{p,q}{}^{RI}(z - z_0), \tag{31}$$

where z_0 is the z coordinate at the beginning of the segment and the β terms are the complex propagation constants of each mode in segment *RI*. In the ideal U-GACC, the phase mismatch between the modes upon traversing each segment is equal to $\pi/2$, resulting in a total phase mismatch of 2π over a full period. Only two unique segment lengths must be calculated, as the real part of the propagation constant is negligibly affected by the gain–loss grating. Segment lengths are thus equal to

$$\Lambda^H = \frac{\pi}{2\,\mathrm{Re}\left(\beta_1{}^H - \beta_2{}^H\right)}, \quad (HH,\ HL \text{ segments}), \tag{32}$$

$$\Lambda^L = \frac{\pi}{2\,\mathrm{Re}\left(\beta_1{}^L - \beta_2{}^L\right)}, \quad (LH,\ LL \text{ segments}), \tag{33}$$

where the superscripts H and L refer to the regions of high and low real index, irrespective of the imaginary index. Here, we note that the TMM analysis has provided a duty cycle for the real grating—defined here as $\Lambda^H/(\Lambda^H + \Lambda^L)$—that differs from 0.5, as is assumed in CMT [11]. In comparison, the duty cycle of the imaginary grating is exactly 0.5, in order to produce zero net gain in each period. The period of the full complex grating is then

$$\Lambda = 2\left(\Lambda^H + \Lambda^L\right). \tag{34}$$

In addition to the phase mismatch, the modes experience gain and loss during propagation, as determined by the imaginary part of the propagation constants. With zero net gain in the ideal device, the gain and loss in segments with the same real index are the inverse of one another. There does exist, however, a slight disparity in gain between segments of high and low real index, due to the difference both in segment lengths and modal overlap with the gain region (this, again, is not accounted for in CMT). The gain of each mode in the segment with high real index is thus denoted

$$g_{p,q}{}^H = \exp\left[\mathrm{Im}\left(\beta_{p,q}{}^H\right)\Lambda^H\right], \tag{35}$$

while that in the segment with low real index is

$$g_{p,q}{}^L = \exp\left[\mathrm{Im}\left(\beta_{p,q}{}^L\right)\Lambda^L\right]. \tag{36}$$

We are now in a position to define the propagation matrix in segment *RI* as

$$\mathbf{P}^{RI} = \begin{bmatrix} \exp\left(-i\phi_1{}^{RI}\right) & 0 \\ 0 & \exp\left(-i\phi_2{}^{RI}\right) \end{bmatrix}. \tag{37}$$

In the grating segments with high real index, the propagation matrices for the ideal U-GACC are

$$\mathbf{P}^{HH} = \begin{bmatrix} g_1{}^H & 0 \\ 0 & ig_2{}^H \end{bmatrix}, \qquad \mathbf{P}^{HL} = \begin{bmatrix} \left(g_1{}^H\right)^{-1} & 0 \\ 0 & i\left(g_2{}^H\right)^{-1} \end{bmatrix}, \tag{38}$$

where a common phase $\exp[-i\,\mathrm{Re}(\beta_1{}^H)\Lambda^H]$ has been factored out without loss of generality. Likewise, in the segments with low real index,

$$\mathbf{P}^{LH} = \begin{bmatrix} g_1{}^L & 0 \\ 0 & ig_2{}^L \end{bmatrix}, \qquad \mathbf{P}^{LL} = \begin{bmatrix} \left(g_1{}^L\right)^{-1} & 0 \\ 0 & i\left(g_2{}^L\right)^{-1} \end{bmatrix}. \tag{39}$$

D. Full-Period Transfer Matrix

For the grating orientation in Fig. 2, the transfer matrix for a full period is

$$\begin{aligned} \mathbf{T} &= \mathbf{T}^{(HH)LH}\mathbf{P}^{LH}\mathbf{T}^{(LH)LL}\mathbf{P}^{LL}\mathbf{T}^{(LL)HL}\mathbf{P}^{HL}\mathbf{T}^{(HL)HH}\mathbf{P}^{HH} \\ &= \begin{bmatrix} T_{11} & T_{12} \\ T_{21} & T_{22} \end{bmatrix}, \end{aligned} \tag{40}$$

where, to second order in all ε terms,

$$T_{11} = 1 - \varepsilon_X{}^2\left(\frac{g_1{}^L}{g_2{}^L} - 2\,\frac{g_1{}^H}{g_2{}^H} - \frac{g_2{}^L}{g_1{}^L} - \frac{g_1{}^L g_1{}^H}{g_2{}^L g_2{}^H} + 1\right), \tag{41}$$

$$T_{12} = -\varepsilon_X\left(\frac{g_2{}^H}{g_1{}^H} + \frac{g_1{}^L}{g_2{}^L} + 2\right), \tag{42}$$

$$T_{21} = -\varepsilon_X\left(\frac{g_1{}^H}{g_2{}^H} + \frac{g_2{}^L}{g_1{}^L} - 2\right), \tag{43}$$

$$T_{22} = 1 - \varepsilon_X{}^2\left(\frac{g_1{}^L}{g_2{}^L} + 2\,\frac{g_2{}^H}{g_1{}^H} - \frac{g_2{}^L}{g_1{}^L} - \frac{g_2{}^L g_2{}^H}{g_1{}^L g_1{}^H} + 1\right). \tag{44}$$

$\mathbf{T}$ is unimodular, as is expected from a system with segments of equal gain and loss when the scattering loss is neglected. However, unlike the transfer matrix

of a pure index grating, $\mathbf{T}$ is not unitary, and as a result, the total optical power changes (and in fact, grows) during propagation. This surprising result occurs because the modes interfere constructively in the regions with gain and destructively in the lossy regions.

The asymmetry in $\mathbf{T}$ is evident from the ratio of off-diagonal terms $|T_{12}|/|T_{21}|$, which is not equal to unity. In Section 4, we shall see that in practical U-GACC designs all gain terms are very slightly greater than unity, and thus the ratios $g_p^{H,L}/g_q^{H,L}$ in Eqs. (41)–(44) are all approximately equal to one. In this case, the single-period transfer matrix can be simplified to

$$\mathbf{T} \approx \begin{bmatrix} 1+2{\varepsilon_X}^2 & -4\varepsilon_X \\ 0 & 1-2{\varepsilon_X}^2 \end{bmatrix}. \tag{45}$$

E. Reversed Grating Phase

The analysis in Subsection 3.D considered a structure in which the gain–loss grating leads the index grating when propagating from left to right. If this grating phase is switched (either by physically reversing the gain and loss segments, or merely by propagating through the structure in the reverse direction), then by Eq. (2), we expect the allowed direction of coupling to be reversed as well. To verify this, we define the reverse single-period transfer matrix $\mathbf{T}_{\text{rev}}$ in the same way as Eq. (40), but with the eight submatrices in the reverse order; superscripts on the transfer matrices between each segment are flipped to indicate the reversed direction of propagation:

$$\mathbf{T}_{\text{rev}} = \mathbf{P}^{HH}\mathbf{T}^{(HH)HL}\mathbf{P}^{HL}\mathbf{T}^{(HL)LL}\mathbf{P}^{LL}\mathbf{T}^{(LL)LH}\mathbf{P}^{LH}\mathbf{T}^{(LH)HH}. \tag{46}$$

We now remark that at each grating plane, from Eq. (15),

$$\mathbf{T}^{(RI)R'I'} = \left(\mathbf{T}^{(R'I')RI}\right)^T. \tag{47}$$

Together with the trivial observation that $(\mathbf{P}^{RI})^T = \mathbf{P}^{RI}$, we can rewrite Eq. (46) as

$$\begin{aligned}\mathbf{T}_{\text{rev}} &= (\mathbf{P}^{HH})^{\mathrm{T}}(\mathbf{T}^{(HL)HH})^{\mathrm{T}}(\mathbf{P}^{HL})^{\mathrm{T}}(\mathbf{T}^{(LL)HL})^{\mathrm{T}}(\mathbf{P}^{LL})^{\mathrm{T}} \\ &\quad\times (\mathbf{T}^{(LH)LL})^{\mathrm{T}}(\mathbf{P}^{LH})^{\mathrm{T}}(\mathbf{T}^{(HH)LH})^{\mathrm{T}} \\ &= (\mathbf{T}^{(HH)LH}\mathbf{P}^{LH}\mathbf{T}^{(LH)LL}\mathbf{P}^{LL}\mathbf{T}^{(LL)HL}\mathbf{P}^{HL}\mathbf{T}^{(HL)HH}\mathbf{P}^{HH})^{\mathrm{T}} \\ &= \mathbf{T}^{\mathrm{T}}. \end{aligned} \tag{48}$$

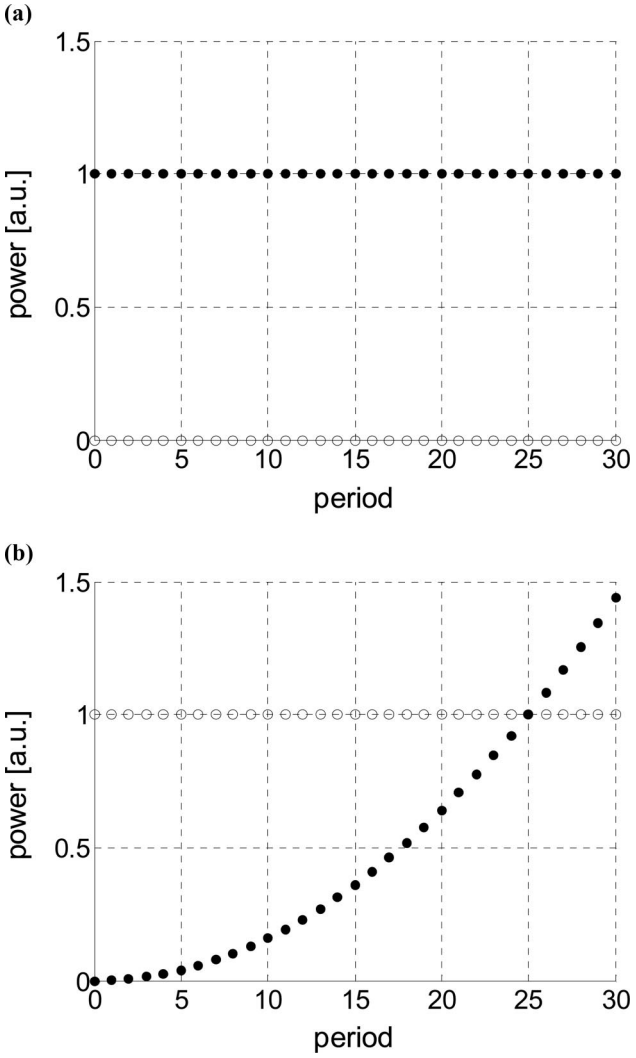

Fig. 3. Modal power evolution in an ideal U-GACC ($2 \rightarrow 1$ coupling permitted, $\varepsilon_X = 0.01$). ●, mode 1; ○, mode 2. (a) Power input to mode 1. (b) Power input to mode 2.

Thus, a U-GACC with reversed phase between the real and imaginary gratings is described by the original transfer matrix with the elements T_{12} and T_{21} exchanged, indicating that the allowed direction of coupling is indeed reversed.

F. N-Period Grating

The unimodular property of $\mathbf{T}$ allows us to apply Chebyshev's formula [14] to determine the transfer matrix of an N-period U-GACC:

$$\mathbf{T}^N = \begin{bmatrix} 1-N{\varepsilon_X}^2\left(\dfrac{g_1^{\,L}}{g_2^{\,L}} - 2\dfrac{g_1^{\,H}}{g_2^{\,H}} - \dfrac{g_2^{\,L}}{g_1^{\,L}} - \dfrac{g_1^{\,L}g_1^{\,H}}{g_2^{\,L}g_2^{\,H}} + 1\right) & -N\varepsilon_X\left(\dfrac{g_2^{\,H}}{g_1^{\,H}} + \dfrac{g_1^{\,L}}{g_2^{\,L}} + 2\right) \\ -N\varepsilon_X\left(\dfrac{g_1^{\,H}}{g_2^{\,H}} + \dfrac{g_2^{\,L}}{g_1^{\,L}} - 2\right) & 1-N{\varepsilon_X}^2\left(\dfrac{g_1^{\,L}}{g_2^{\,L}} + 2\dfrac{g_2^{\,H}}{g_1^{\,H}} - \dfrac{g_2^{\,L}}{g_1^{\,L}} - \dfrac{g_2^{\,L}g_2^{\,H}}{g_1^{\,L}g_1^{\,H}} + 1\right) \end{bmatrix}. \tag{49}$$

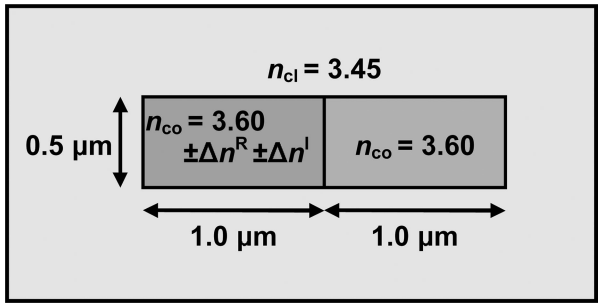

Fig. 4. Cross section of example U-GACC analyzed in this work. $\Delta n^R = \Delta n^I = 5 \times 10^{-4}$.

When all gain ratios ${g_p}^{H,L}/{g_q}^{H,L}$ are assumed equal to unity as in Eq. (45), this simplifies to

$$\mathbf{T}^N = \begin{bmatrix} 1 + 2N{\varepsilon_X}^2 & -4N\varepsilon_X \\ 0 & 1 - 2N{\varepsilon_X}^2 \end{bmatrix} \approx \begin{bmatrix} 1 & -4N\varepsilon_X \\ 0 & 1 \end{bmatrix}, \tag{50}$$

where the approximation assumes that $\varepsilon_X \ll 2$. From Eq. (3), the electric field amplitudes of the modes at the end of the grating are therefore

$$\begin{bmatrix} {E_1}^{\text{out}} \\ {E_2}^{\text{out}} \end{bmatrix} = \mathbf{T}^N \begin{bmatrix} {E_1}^{\text{in}} \\ {E_2}^{\text{in}} \end{bmatrix} = \begin{bmatrix} {E_1}^{\text{in}} - 4N\varepsilon_X {E_2}^{\text{in}} \\ {E_2}^{\text{in}} \end{bmatrix}. \tag{51}$$

Figure 3 illustrates the evolution of modal power in a hypothetical U-GACC for which only coupling from mode 2 to mode 1 is allowed, with $\varepsilon_X = 0.01$. Note that the linear increase in coupled field magnitude [see T_{12} of Eq. (51)] results in a quadratic increase in coupled power. The number of periods required to achieve equalization (at a minimum) of field magnitude in the two modes is determined by setting $|T_{12}| = 1$,

$$N_{\text{eq}} = \left\lceil \frac{1}{4\varepsilon_X} \right\rceil, \tag{52}$$

where the ceiling function $\lceil \cdot \rceil$ is used to indicate that N_{eq} must be an integer.

G. Cross Talk

A U-GACC will exhibit a finite cross talk according to Eq. (49), as $|T_{21}|$ is not precisely zero. If we define the cross talk as the ratio of power leakage in the forbidden direction to power coupling in the allowed direction (for identical mode amplitudes input to the grating), it can be expressed simply as

$$\text{cross talk} = |T_{21}/T_{12}|^2 = \left| \frac{({g_1}^H/{g_2}^H) + ({g_2}^L/{g_1}^L) - 2}{({g_2}^H/{g_1}^H) + ({g_1}^L/{g_2}^L) + 2} \right|^2, \tag{53}$$

irrespective of the number of grating periods, with T_{21} and T_{12} exchanged in the case of reversed grating phase.

4. Example

To demonstrate the TMM, we consider the structure outlined in Figs. 2 and 4. This U-GACC is designed for operation at $\lambda = 1.55$ μm, and consists of a dual-mode waveguide with rectangular core of 0.5 μm height and 2.0 μm width. The unperturbed refractive indices are 3.60 (core) and 3.45 (cladding). Index perturbations Δn^{R} and Δn^{I} are $\pm 5 \times 10^{-4}$ within the left half of the core cross section and zero within the right half. As the real and imaginary perturbations are spatially colocated in this example, their magnitudes will be equal in the ideal U-GACC case.

Mode profiles and propagation constants are calculated using a semivectorial finite difference method [15] with variable node spacing [16]; quasi-TE modes (those with dominant electric field component parallel to the long axis of the core) are considered here. Table 1 contains calculated complex effective indices for both modes in each segment, as well as the segment length corresponding to $\pi/2$ phase mismatch between modes [Eqs. (32) and (33)], and the gain of the modes in each segment [Eqs. (35) and (36)]. The magnitude of the off-diagonal term in each individual transfer matrix is calculated to be $\varepsilon_X = 0.00733$ [Eqs. (24) and (29)].

Using Eqs. (41)–(44), the transfer matrix for a single period of this U-GACC is found to be

$$\mathbf{T} = \begin{bmatrix} 1.000106 & -2.91 \times 10^{-2} \\ -1.13 \times 10^{-6} & 0.999894 \end{bmatrix}. \tag{54}$$

The 4 orders of magnitude difference between T_{12} and T_{21} indicates a very strong asymmetry in the coupling

Table 1. Calculated Effective Mode Indices, Segment Lengths, and Segment Gain for the Example in Section 4

Segment and Mode	n_{eff}	Λ (μm) [from Eqs. (32)–(33)]	Gain [from Eqs. (35)–(36)]
HH, 1	$3.509038 + (1.70952 \times 10^{-4})i$		${g_1}^H = 1.00764$
HH, 2	$3.473577 + (1.39386 \times 10^{-4})i$	$\Lambda^H = 10.928$	${g_2}^H = 1.00624$
HL, 1	$3.509038 - (1.70952 \times 10^{-4})i$		
HL, 2	$3.473577 - (1.39386 \times 10^{-4})i$		
LL, 1	$3.508698 - (1.68441 \times 10^{-4})i$		${g_1}^L = 1.00754$
LL, 2	$3.473298 - (1.40371 \times 10^{-4})i$		${g_2}^L = 1.00630$
LH, 1	$3.508698 + (1.68441 \times 10^{-4})i$	$\Lambda^L = 10.946$	
LH, 2	$3.473298 + (1.40371 \times 10^{-4})i$		

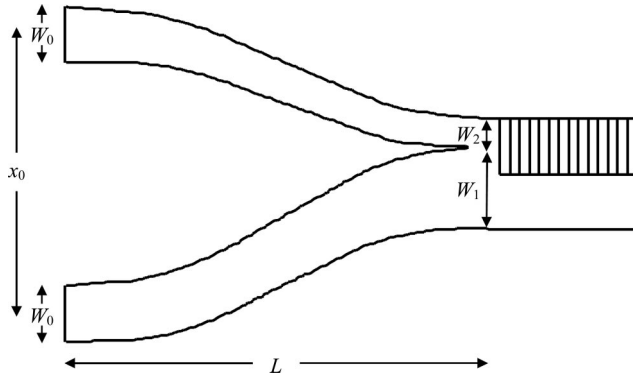

Fig. 5. Geometry of the adiabatic asymmetric y-branch multiplexer.

characteristics of this structure. From Eq. (52), field equalization in both modes is achieved after 35 periods of the grating. Finally, we note that the duty cycle of this ideal U-GACC is 0.4996, due to the slightly larger discrepancy between mode indices in the segments with high real index. This differs negligibly from 0.5, but it should be noted that the departure from a 0.5 duty cycle is considerably larger for the geometry shown in Fig. 1. The cross talk, by Eq. (53), is −44 dB, which can be considered negligible in comparison to that which is incurred in demultiplexing the two modes at the end of the grating.

To verify these results, we simulate this 35-period U-GACC using a three-dimensional beam propagation method (BPM) [17]. The adiabatic asymmetric y-branch used to multiplex signals from two input waveguides onto the two guided modes utilizes tapered sinusoidal s-bends (see Fig. 5). It has length $L = 500$ μm and initial waveguide separation $x_0 = 5$ μm. Both waveguides have initial width $W_0 = 1$ μm, and final waveguide widths are $W_1 = 1.5$ μm (coupling to mode 1) and $W_2 = 0.5$ μm (coupling to mode 2). The demultiplexing y-branch is identical.

Figure 6 shows the power profile along the U-GACC and at the output plane of the demultiplexer. The figures in the top row describe a grating with segments ordered *HH*, *HL*, *LL*, *LH*. With optical power input to mode 2 (top left figure), the output powers in each mode are approximately identical. Optical power input to mode 1 (top right figure) remains in that mode. In the bottom row, the order of segments is inverted: *HH*, *LH*, *LL*, *HL*. In this case, the coupling properties are reversed, as explained in Subsection 3.E. The modal power at the end of each period for the U-GACC with coupling from mode 2 to

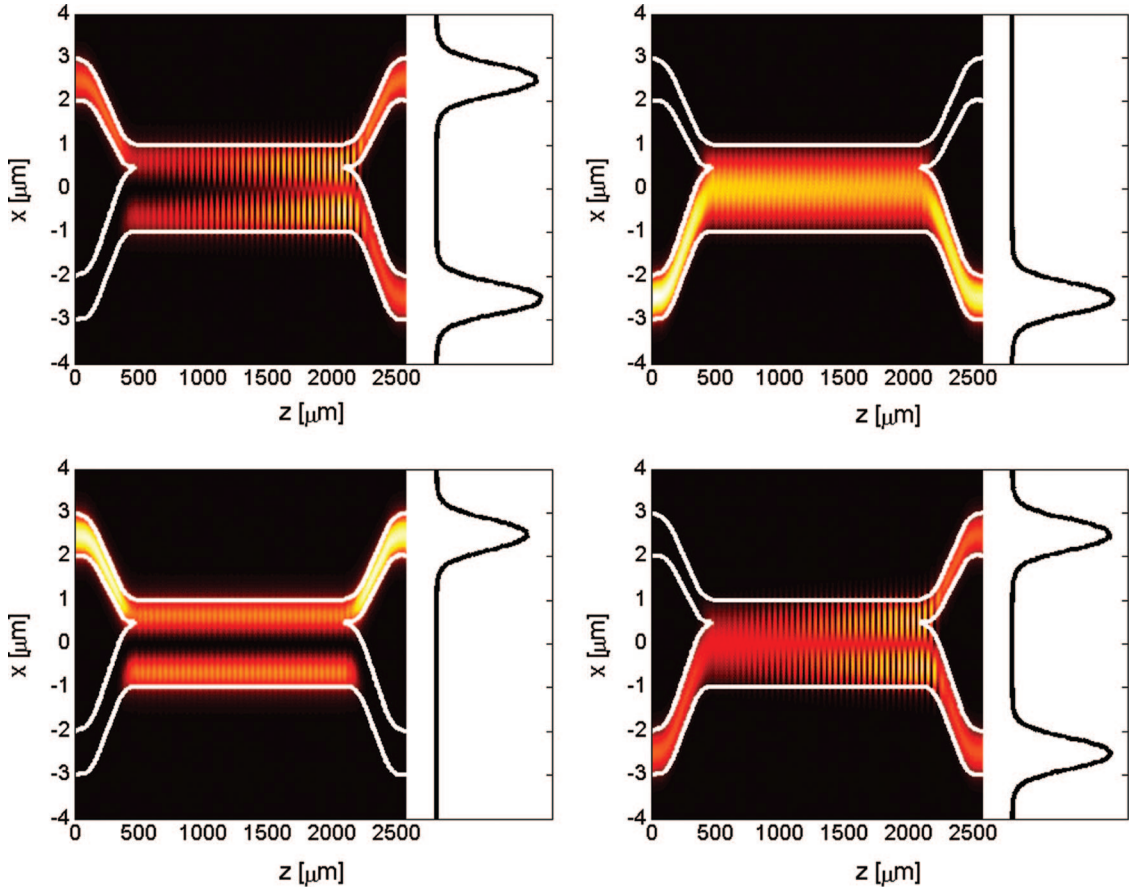

Fig. 6. (Color online) Optical power in the U-GACC example from Section 4. Top row, order of grating segments: *HH*, *HL*, *LL*, *LH*. Bottom row, order of grating segments: *HH*, *LH*, *LL*, *HL*. Left column, power input to mode 2. Right column, power input to mode 1. The curves to the right of each plot show the power at the output plane of the demultiplexer (arbitrary units).

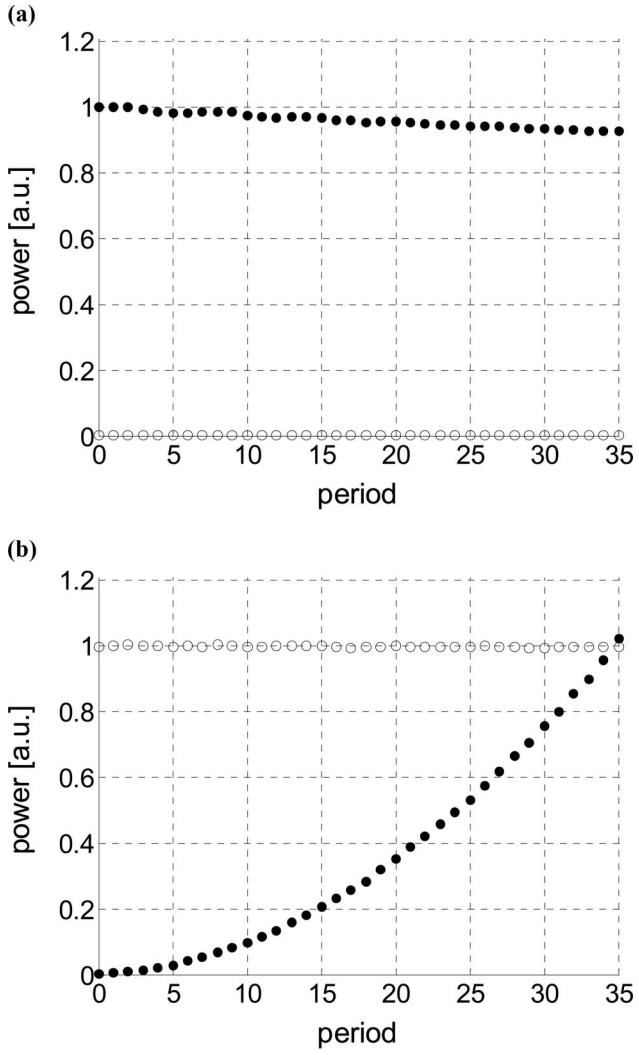

Fig. 7. Modal power evolution in the U-GACC example of Section 4. Order of grating segments: *HH*, *HL*, *LL*, *LH*. ●, mode 1; ○, mode 2. (a) Power input to mode 1: see Fig. 6, upper right figure. (b) Power input to mode 2: see Fig. 6, upper left figure.

mode 1 permitted is shown in Fig. 7. As predicted by Eq. (52), power is equalized by the end of the 35th period of the grating. It is also apparent from this figure that there is scattering present, and that it is more prevalent for mode 1 than for mode 2; this is likely due to the fact that mode 1 has peak power at the index discontinuity at $x = 0$, whereas mode 2 has a null along this axis.

5. Conclusion

The ideal unidirectional grating-assisted codirectional coupler has been analyzed by the transfer matrix method, which demonstrates clearly why such a device exhibits such a strong asymmetry in modal coupling. Simple formulas are found to calculate the number of grating periods required for equalization of modal power, and for the cross talk, which is shown to be finite. These have been confirmed by comparison with BPM simulations. Although this work concerns the ideal structure, nonidealities can easily be analyzed by using the explicit (nonsimplified) matrices to describe scattering between grating planes [Eq. (15)] and propagation within each grating segment [Eq. (37)]. In addition, it should be pointed out that the introduction of the perturbation fields in Eq. (7) was done in order to facilitate the derivation of the transfer matrix elements. In practical application of this work, these matrix elements would be calculated explicitly using Eq. (15).

This work was supported by the Natural Sciences and Engineering Research Council (NSERC) and industrial and government partners, through the Agile All-Photonic Networks (AAPN) Research Network.

References

1. D. Marcuse, "Directional couplers made of nonidentical asymmetrical slabs. Part II: grating-assisted couplers," J. Lightwave Technol. **LT-5,** 268–273 (1987).
2. A. Yariv and M. Nakamura, "Periodic structures for integrated optics," IEEE J. Quantum Electron. **QE-13,** 233–253 (1977).
3. D. Marcuse, *Theory of Dielectric Optical Waveguides* (Academic, 1991).
4. M. Greenberg and M. Orenstein, "Irreversible coupling by use of dissipative optics," Opt. Lett. **29,** 451–453 (2004).
5. T. Galstian, "Non-reciprocal optical element for photonic devices," U.S. patent 6,611,644 B2 (23 August 2003).
6. M. Greenberg and M. Orenstein, "Filterless 'add' multiplexer based on novel complex gratings assisted coupler," IEEE Photon. Technol. Lett. **17,** 1450–1452 (2005).
7. M. Greenberg, "Unidirectional mode devices based on irreversible mode coupling," M.Sc. thesis (Israel Institute of Technology, 2004).
8. M. Kulishov, J. M. Laniel, N. Belanger, and D. V. Plant, "Trapping light in a ring resonator using a grating-assisted coupler with asymmetric transmission," Opt. Express **13,** 3567–3578 (2005).
9. L. Poladian, "Resonance mode expansions and exact solutions for nonuniform gratings," Phys. Rev. E **54,** 2963–2975 (1996).
10. M. Kulishov, J. M. Laniel, N. Belanger, J. Azana, and D. V. Plant, "Nonreciprocal waveguide Bragg gratings," Opt. Express **13,** 3068–3078 (2005).
11. M. Greenberg and M. Orenstein, "Optical unidirectional devices by complex spatial single sideband perturbation," IEEE J. Quantum Electron. **41,** 1013–1023 (2005).
12. W. Huang and J. Hong, "A transfer matrix approach based on local normal modes for coupled waveguides with periodic perturbations," J. Lightwave Technol. **10,** 1367–1375 (1992).
13. W. K. Burns and A. F. Milton, "Mode conversion in planar-dielectric separating waveguides," IEEE J. Quantum Electron. **QE-11,** 32–39 (1975).
14. M. Born and E. Wolf, *Principles of Optics: Electromagnetic Theory of Propagation, Interference, and Diffraction of Light,* 6th ed. (Pergamon, 1980).
15. M. S. Stern, "Semivectorial polarised finite difference method for optical waveguides with arbitrary index profiles," IEE Proc.-J.: Optoelectron. **135,** 56–63 (1988).
16. C. M. Kim and R. V. Ramaswamy, "Modeling of graded-index channel waveguides using nonuniform finite difference method," J. Lightwave Technol. **7,** 1581–1589 (1989).
17. Optiwave Systems, Inc., OptiBPM v. 8.1, http://www.optiwave.com.